Strain measurement in tapered optical fiber sensors with deep learning using speckle pattern imaging

HUSAMETTIN SERBETCI[1,2,*], ISA NAVRUZ[3], FIKRET ARI[3]
[1]*Graduate School of Natural and Applied Sciences, Ankara University, 06110 Ankara, Turkey*
[2]*Department of Electrical and Electronics Engineering, Cankiri Karatekin University, 18100 Cankiri, Turkey*
[3]*Department of Electrical and Electronics Engineering, Ankara University, 06100 Ankara, Turkey*

In this study, a low-cost and compact tapered optical fiber (TOF) sensor for strain measurement was proposed and experimentally demonstrated. It has been proven that the speckle pattern images recorded with a CCD camera at the fiber output are highly sensitive to the strain applied to the sensor region, and therefore the proposed sensor can measure at a very high resolution of 12.5 με. The effect of sensor geometry on sensor sensitivity was investigated through correlation analysis, and it was shown that sensor sensitivity increased with decreasing waist diameter and increasing waist length of the TOF sensor. In the training of the dataset, real data obtained from experimental studies were used and a strain detection architecture based on convolutional neural networks (CNN) was developed. A high-resolution and high-sensitivity fiber sensor capable of measuring strain with high accuracy has been developed using deep learning network.

(Received August 12, 2024; accepted February 3, 2025)

Keywords: Optical fiber sensor, Tapered optical fiber, Speckle pattern, Strain, Deep learning, CNN

1. Introduction

Strain is a significant physical quantity used to determine the endurance, reliability, and mechanical properties of a material. Strain measurement plays a crucial role in construction, aerospace, biomedical, and many other scientific and industrial fields. In recent years, many methods such as FBG [1-3], Fabry–Perot Interferometer [4-6], Polarimetric sensors [7] Mach–Zehnder interferometer [8-11] and TOF sensors [8, 12-16] have been proposed for strain measurement with fiber optic sensors. It is possible to make more sensitive and high-resolution measurements, in comparison with all these methods, using TOF sensors due to the advantages of the deformation in the geometric structure of the optical fiber. In traditional methods, the detection process is carried out by analyzing the shifts in the wavelength spectrum of the guided modes in the fiber with an optical spectrum analyzer (OSA).

An alternative and innovative approach can be introduced in TOF sensors to enable strain detection using speckle patterns. A low-cost and compact sensor can be produced by using a CCD camera instead of an OSA. Speckle patterns are an interference pattern that occurs depending on the amplitude, phase, and wavelength of the guided modes in the fiber. In speckle pattern-based fiber sensors, the detection relies on analyzing the recorded images at the fiber output by using image processing techniques to measure the physical quantity. The relationship between speckle pattern images for the measurement of physical quantities has been investigated in the literature through methods such as normalized intensity inner product coefficient [17], machine learning [18, 19], correlation coefficient (CC) [20], and deep learning [21-24].

In this study, a TOF sensor is proposed for strain measurement, and the effects of the geometric parameters of the sensor on sensitivity are investigated. The measurement sensitivity changes as the waist diameter and length of the sensor region are altered. Therefore, experiments were carried out using sensors with different waist diameters and lengths. Through experimental studies, it has been observed that reducing the waist diameter and increasing the waist length result in an improvement in sensitivity. In the literature review, no study was found that used speckle pattern images to measure strain in TOF sensors. Therefore, this study introduces a novel approach to strain measurement in TOF sensors by using speckle pattern images trained with a deep learning network. In addition to strain measurement, it is also possible to measure various physical quantities such as refractive index [15, 20, 25], temperature [16], magnetic field [26], and displacement [27, 28] with the proposed sensor structure.

2. Theory

When the part of the optical fiber to be used for the sensor is tapered below the penetration depth, the guided modes will reflect from the surrounding medium. In this case, shifts occur in the wavelength spectrum of the guided modes, and these shifts are analyzed by OSA. In this study, the detection was performed using the proposed speckle pattern imaging method as an alternative to using an OSA. The optical fiber, illuminated by a laser light source, excites hundreds of linearly polarized modes. Due to the different amplitude and phase of each guided mode, a random intensity distribution of light, known as a speckle pattern, is formed at the fiber output. The interference of the complex fields of all guided linear polarized modes gives the complex speckle pattern field, and is calculated with Equation 1.

$$A(x,y) = \sum_{m=0}^{M} a_m(x,y)\exp[j\varphi_m(x,y)] \quad (1)$$

Here, $a_m(x,y)$ and $\varphi_m(x,y)$ represent the amplitude and phase of the m-th mode, respectively. The light intensity of the speckle pattern formed in the x-y plane is expressed by Equation 2 [17].

$$I(x,y) = \sum_{m=0}^{M}\sum_{n=0}^{M} a_m a_n \exp[\mathrm{j}(\varphi_m - \varphi_n)] \quad (2)$$

Physical quantities such as temperature, strain, and magnetic field applied to the part of the fiber intended for sensor purposes will cause variations in the speckle pattern images. In speckle pattern imaging-based fiber sensors, the detection process is performed by analyzing the changes occurring in the images. In order to establish the relationship between speckle patterns and strain, the quantitative value of strain needs to be determined. The strain's quantitative values ε is expressed as the change in the longitudinal length per unit length of the fiber, as shown in Equation 3.

$$\varepsilon = \frac{\Delta L}{L} \quad (3)$$

In Equation 3, ΔL represents the length change in the fiber due to strain, and L represents the initial length of the fiber. In the experimental studies to be conducted, the changes in the similarity ratio of speckle pattern images will be examined with respect to $\Delta\varepsilon$. The strains applied to the waist region of the TOF sensor will alter the effective refractive index in that region. This change in the effective refractive index will lead to a phase difference between the modes propagating in the core and cladding, resulting in variations in the speckle pattern images proportional to the applied strain [8].

3. Material and method

3.1. Fabrication of TOF sensor

The waist length and diameter of the TOF sensor are among the most crucial parameters affecting the sensitivity of the sensor. Therefore, these parameters should be selected at optimum values during the fabrication of the sensor. A fabrication setup shown in Fig. 1 has been developed to produce sensors with the desired waist length and diameter. The part of the optical fiber to be tapered is placed between two fiber holders, with a distance of 20 cm between them, where one is fixed and the other is placed on a linear translation stage (LTS). The optical fiber is heated by the electric arc produced between a pair of electrodes placed on another LTS. When the fiber reaches the softening temperature (approximately 2-3 seconds), the movable holder begins to pull the fiber. At this stage, the other LTS moves the position of its electrodes in the opposite direction from the pull direction. During the TOF sensor fabrication, a computer controls many parameters, such as the speed and acceleration of the stepper motors driving the LTSs and the arc power and time duration of the pulse signal applied to the electrodes. This way, biconical tapered fiber is successfully fabricated with the desired waist diameter and waist length.

We fabricated TOF sensors with waist diameters of 10 to 35 µm and waist lengths of 1 to 3.5 cm using SI-MMF. Some microscope images of the fabricated sensors are given in Fig. 2. In our previous study [20], where we performed refractive index measurements, both simulations and experimental studies demonstrated that reducing the waist diameter and increasing the waist length enhanced sensor sensitivity. In this study, the effects of these sensor parameters on strain measurement are investigated.

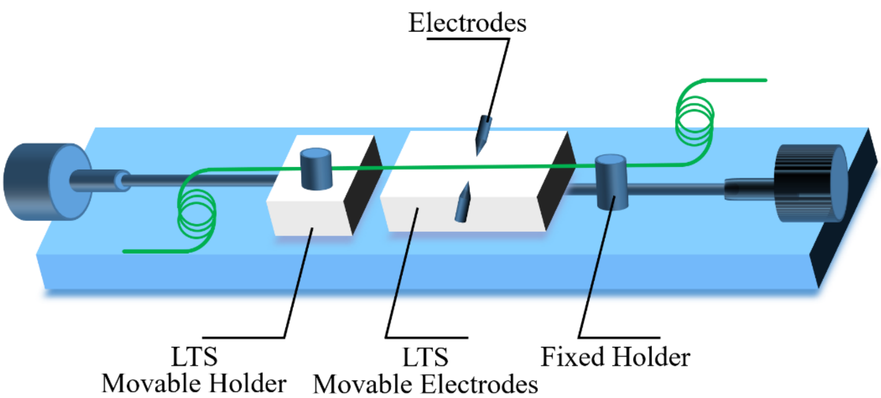

Fig. 1. Illustration of the TOF sensor's fabrication setup (colour online)

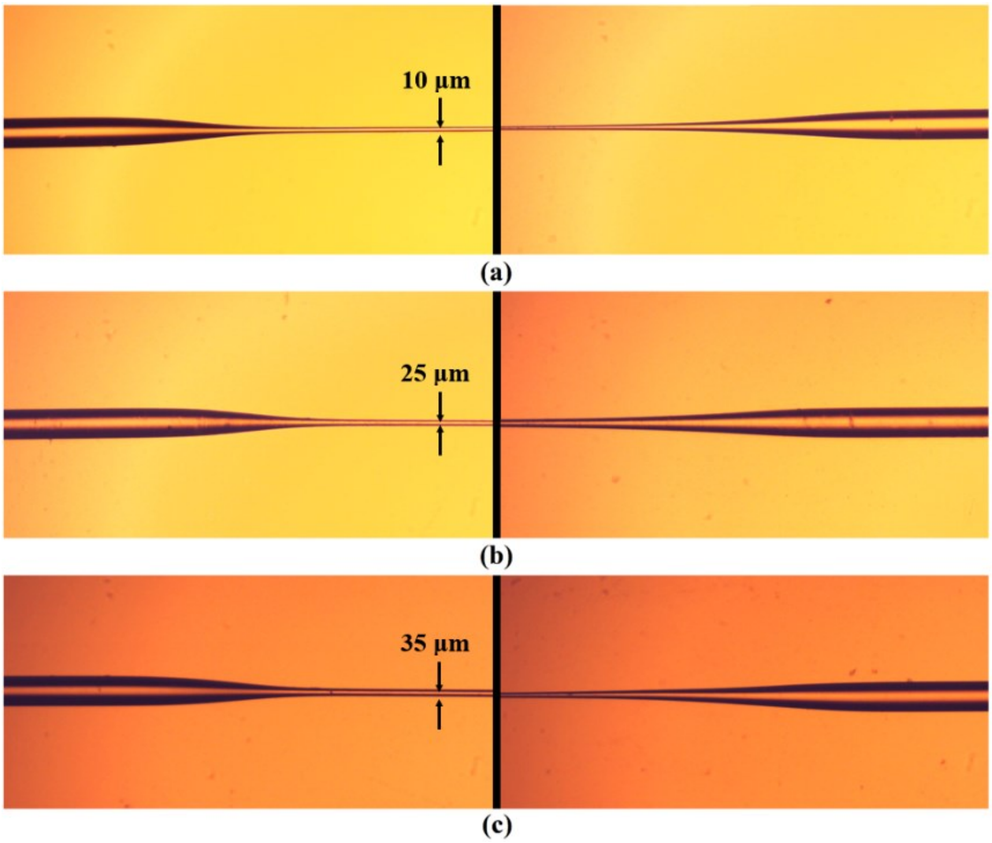

Fig. 2. Microscope images of fabricated TOF sensors (a) 10 µm, (b) 25 µm, (c) 35 µm (colour online)

3.2. Experimental studies

The fabrication setup was used to measure the sensitivity of TOF sensors to strain variation. The sensor was placed on the LTS with the electrodes on it, but the electrodes were left inactive. The fiber sensor was fixed between two fiber holders with at a distance of 20 cm, and then strain was applied by gradually pulling it from the movable end. The movable stage has a minimum step size of 1.25 µm. A picture of the measuring setup is given in Fig. 3. The measurement setup consists of a manual X-Y-Z stage, an optical fiber (Nufern MMF-S105), a laser source (Thorlabs LDM635), and a CCD camera (Thorlabs BC106-VIS). The speckle pattern image formed at the output of the fiber varies depending on the applied strain at each step of the movable stage. These images captured by the CCD camera are analyzed to detect strain.

At 25 °C room temperature, we fixed the fiber by hanging a 2 g weight on one end of the fiber and tried to keep the initial conditions constant. By repeating the experimental studies on the same fiber sensor, we made sure that we were measuring within the fiber's elasticity limits. The sensor region fixed between the two fiber holders was pulled by 10 motor steps (equivalent to 62.5 με) of the movable fiber holder at each stretching step. When the longitudinal strain reached 1250 με, the movable fiber holder moved in the opposite direction with the same step intervals and returned to its initial position. This procedure was repeated five times for each fabricated sensor. In each experiment, 41 speckle pattern images were recorded, and the speckle pattern image at the maximum strain quantity (1250 με) was selected as the reference image.

In experimental studies, we focused on investigating the effect of waist diameter and waist length on sensor sensitivity. Therefore, many fiber sensors with different waist diameters and different waist lengths have been fabricated. Initially, the waist diameter was kept constant at 25 µm and the waist length was changed between 1-3.5 cm. Then, for a fixed waist length of 2.25 cm, the waist diameter was changed in the range of 10-35 µm. To test the strain sensitivity of each sensor, the correlation between the speckle pattern images captured by the camera was analyzed by calculating CCs. The CCs corresponding to the same longitudinal strains in the ±x directions were close to each other as expected, which indicated that the experiments were consistent, and that the fiber was pulled within elastic limits. The consistency of the results indicated that the images could be used for strain detection with CNN.

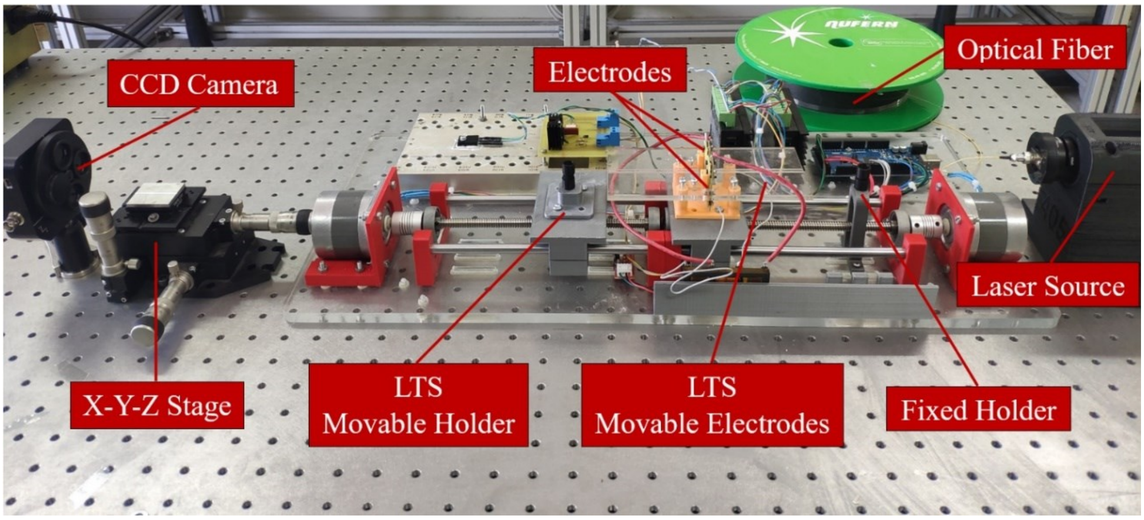

Fig. 3. Fabrication setup of TOF sensor (colour online)

3.3. Correlation analysis and CNN

It would be helpful to pre-process the recorded speckle pattern images before the correlation analysis. Due to the cylindrical structure of the fiber, the speckle pattern images are formed within a circle on the camera. To eliminate any impact of the outer region on correlation, the outer area was masked, and then the area where the patterns were formed was cropped. Finally, background correction was applied to eliminate non-uniform illumination and increase speckle visibility. This process rendered the images ready for correlation analysis. An illustration of these processes is shown in Fig. 4.

The similarity relationship between two images can be investigated using the correlation coefficient, denoted by CC, given in Equation 4.

$$CC = \frac{\sum(M_i - \bar{M})(N_i - \bar{N})}{\sqrt{\sum(M_i - \bar{M})^2 \sum(N_i - \bar{N})^2}} \quad (4)$$

M_i and N_i represent the reference image and the other image to be correlated, respectively, while $\bar{M}$ and $\bar{N}$ represent the mean of these images. The calculation of correlation between the two images can be improved by dividing these images into segments instead of processing entire images. Therefore, we divided the background corrected images into 110×110 segments by shifting the rows and columns by 10 pixels, respectively [20].

After showing the sensing performance of our TOF sensors with different parameters by using correlation analysis, a CNN was created to perform strain detection. The CNN consists of an input layer, a convolutional layer, a rectified linear unit (ReLU), a pooling layer, a fully connected layer, a softmax, and a classification layer. The illustration of the CNN is shown in Fig. 5. The selection of parameters and optimization algorithm plays a crucial role in the accuracy of a deep learning algorithm. In this study, sgdm was used as the optimization algorithm while training the CNN. The number of epochs was set to 100, and a minibatch size of 30 was chosen to better manage the training process. The initial learning rate was set to 0.001.

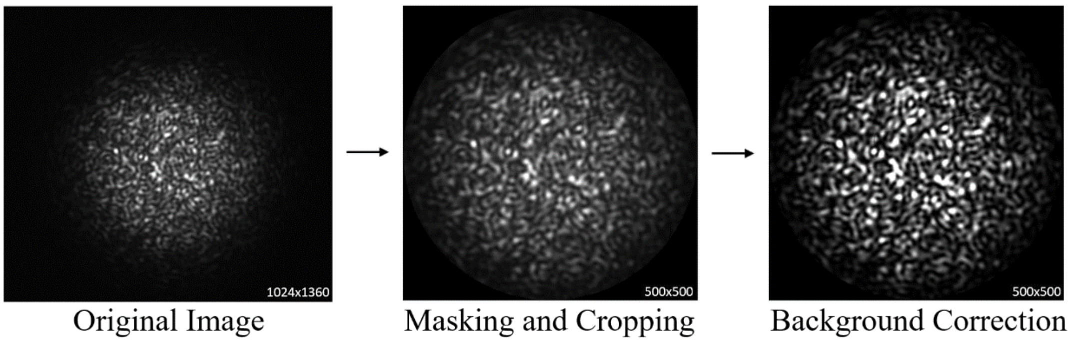

Fig. 4. Illustration of image processing steps

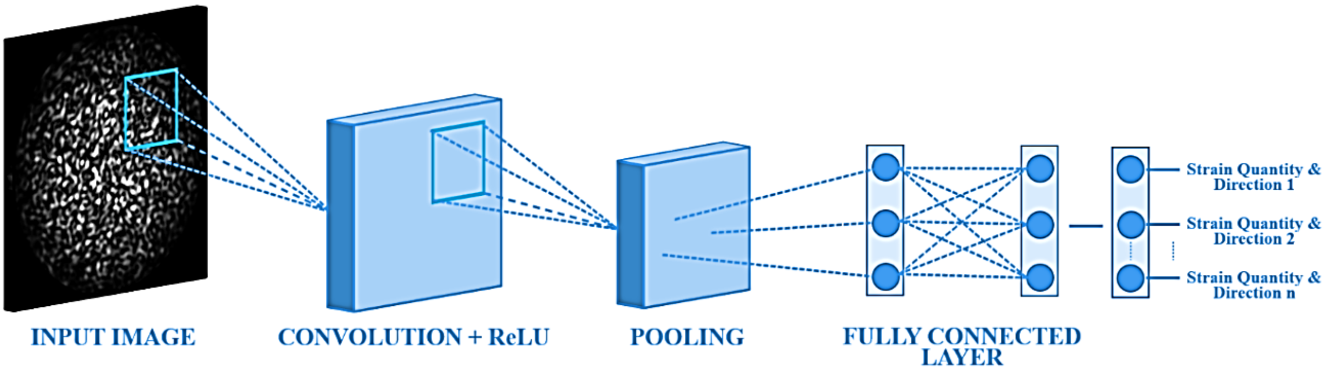

Fig. 5. CNN structure used in this study (colour online)

4. Results

Correlation analysis was performed to examine variation in the speckle pattern images and, the effects of the sensor parameters on the sensitivity. First, experiments were carried out on sensors with a waist diameter of 25 μm and a waist length of 1-3.5 cm. The image corresponding to the maximum strain quantity of 1250 με was chosen as the reference image. Each experiment was repeated five times, and the average CC was calculated. The obtained results are given in Fig. 6.

In tapered optical fibers, as the guiding condition changes, the geometry of the sensor region significantly affects the amplitude and phase of the optical modes. As a result of the strain applied to the sensor, the effective refractive index in the tapered fiber changes, leading to a phase difference between the guided modes in the core and the cladding to change [8]. This change leads to variations in the speckle pattern. When Fig. 6 is examined, it is observed that as the waist length of the sensor increases, the calculated correlation change (ΔCC) for a measurement point (for example, 1125 με) increases. We can define the decoration ratio as ΔCC /Δε. It is clearly seen in the figure that ΔCC /Δε increases as waist length increases. This indicates an increase in sensor sensitivity.

Secondly, the effect of waist diameter on sensor sensitivity was investigated. The experiments were repeated for TOF sensors fixed at a waist length of 2.25 cm and a waist diameter of 10-35 μm. The obtained results are presented in Fig. 7.

Similar to the effect of waist length, the guiding conditions in the sensor region change as the waist diameter changes. As the waist diameter gradually decreases, the higher order modes in the tapered region weaken at the core-cladding interface as they penetrate into the external environment. It can be observed in Fig. 7 that as the waist diameter decreases, the decorrelation rate increases, resulting in an increase in sensor sensitivity. For example, the decorrelation ratio for non-tapered fiber is approximately calculated as 0.48. This ratio is approximately calculated as 1.06 and 6.80 for sensors with waist diameters of 35 and 10 μm, respectively.

In measurements made with 62.5 με strain steps, ΔCC for the fiber with a waist diameter of 20 μm was calculated to be approximately 0.7. This value is approximately 0.8 for the sensor with a waist diameter of 10 μm. This shows that fiber sensors with sufficiently small waist diameters are capable of measuring strain changes smaller than 62.5 με. Therefore, the experiments were repeated for waist diameters 20 μm and 10 μm, applying strain increments of 2 motor steps (corresponding to 12.5 με). The obtained results are presented in Fig. 8.

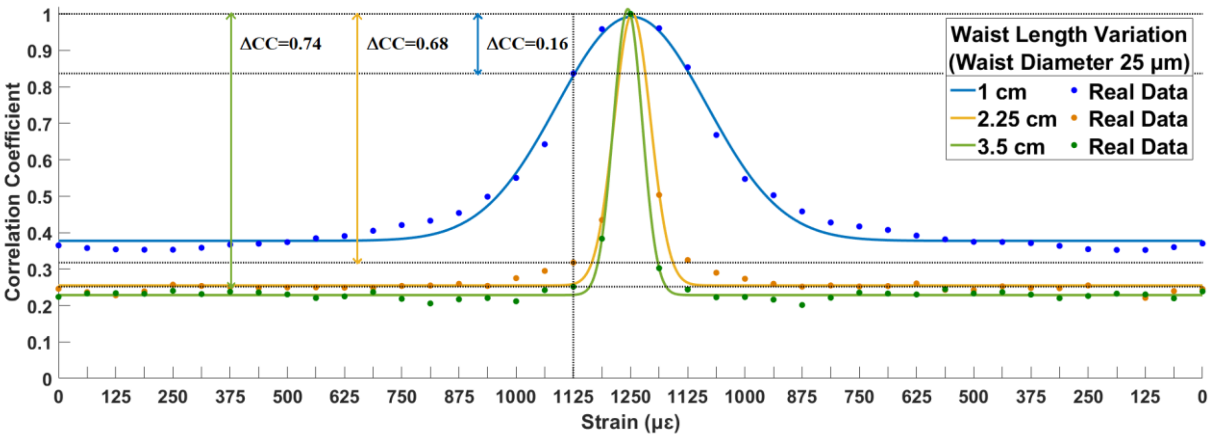

Fig. 6. Correlation coefficient as a function of strain for different waist lengths (colour online)

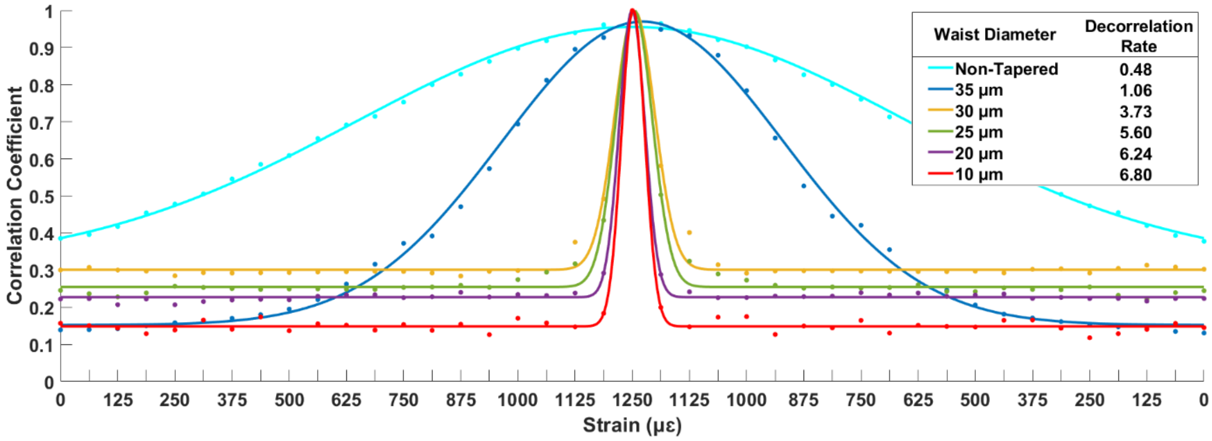

Fig. 7. Correlation coefficient as a function of strain for different waist diameters (colour online)

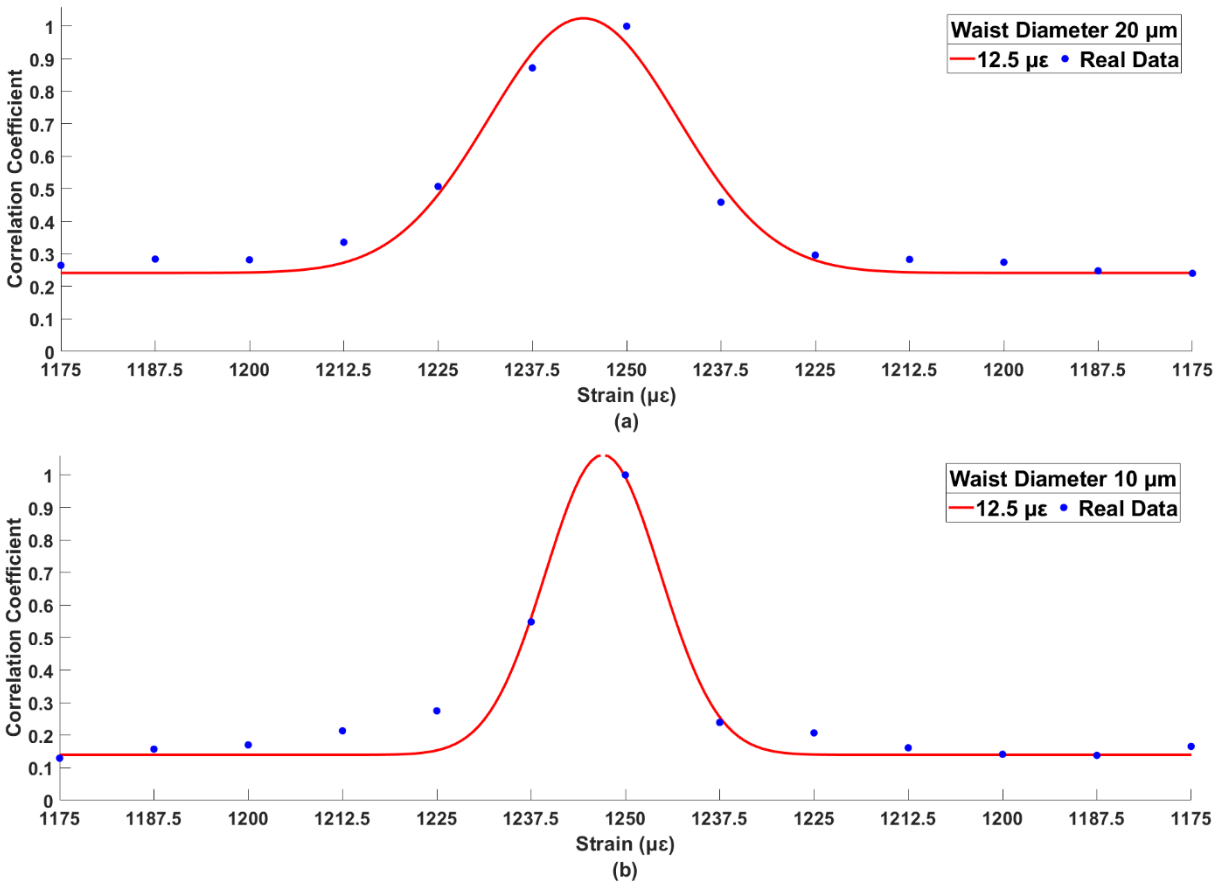

Fig. 8. Correlation coefficients for different strain variations, waist diameter of (a) 20 μm, (b) 10 μm (colour online)

These results prove that our sensor can measure strain changes as small as 12.5 με. Through the experimental studies and correlation analysis of the speckle pattern images, it is observed that the resolution of the sensor and sensitivity increase with an increase in waist length and a decrease in waist diameter. The sensitivity of the sensor to strain was confirmed by correlation analysis, and the effect of waist diameter and length on sensor performance was also determined.

To validate the inferences derived from experimental results and enhance the predictability of measurement outcomes, a CNN has been created for fiber sensors with waist diameters of 125 μm (non-tapered), 35 μm, and 10 μm. In addition to the dataset obtained for strain increments of 62.5 με and 12.5 με, experiments were conducted with strain increments of 43.75 με and 31.25 με, which were not used in the correlation analysis. 41 speckle pattern images were recorded for each experiment, and so 205 images were obtained from repeated experiments. One of these experiments was reserved for testing. The remaining 164 images were rotated 0.5 degrees clockwise and counterclockwise to simulate potential movements in the fiber and expand the data set. Thus, the total number of images increased to 492. From these images, 82 were allocated for validation and the remaining images were used in the training of the CNN model. To be able to determine not only the strain quantity but also the direction of the applied strain, 41 different classes were created. The validation and test accuracy for waist diameter is given in Table 1. To illustrate the training of the CNN, Fig. 9 shows the accuracy and loss of the training and validation as a function of epochs. Accuracy converges to 100% after approximately 90 epochs.

Table 1. Validation and test accuracy for waist diameter variation

Step of Strain	125 μm (Non-Tapered)		35 μm		10 μm	
	Val. (%)	Test (%)	Val. (%)	Test (%)	Val. (%)	Test (%)
62.5 με	82.93	78.05	100	100	100	100
43.75 με	Untried	Untried	97.56	95.12	100	100
31.25 με	Untried	Untried	80.48	73.17	100	100
12.5 με	Untried	Untried	Untried	Untried	93.44	88.52

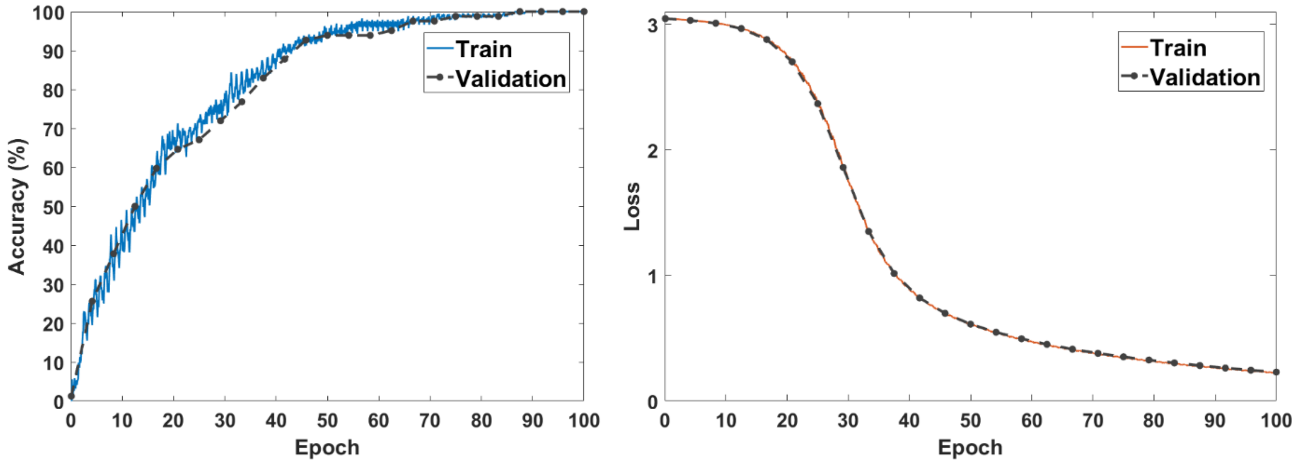

Fig. 9. Accuracy and loss of the training and validation as a function of epochs (colour online)

In the correlation analysis, it was observed that the decrease in waist diameter increases the rate of change in speckle pattern images. When Table 1 is examined, it can be observed that the non-tapered fiber has a low decorrelation rate, which results in lower performance of the CNN compared to the tapered sensors. When examining Table 1, it can be seen that for the non-tapered fiber, decorrelation rate of speckle pattern images is quite high, and therefore, the accuracy rates of the CNN are lower compared to tapered sensors. For the non-tapered fiber, the validation accuracy rate is 82.93%, and the test accuracy rate is 78.05%. For a sensor with a 35 μm waist diameter, the validation and test accuracy rates are 100% for 62.5 με, 97.56% and 95.12% for 43.75 με, 80.48% and 73.17% for 31.25 με values. In experiments conducted with a 10 μm waist diameter sensor, the validation and test accuracy rates are 100% for 62.5 με strain, 100% for 43.75 με, 100% for 31.25 με, and 93.44% and 88.52% for 12.5 με. These results show that a reduction in waist diameter increases the rate of change in speckle pattern and thus leading to more sensitive and high-resolution measurements. Both correlation analysis and CNN confirm this result.

5. Conclusions

In this study, a TOF sensor that measures strain was produced and experimentally tested by using speckle pattern images recorded with a CCD camera instead of OSA. The fabricated sensor can measure strain increments and decrements of 12.5 με with high precision. Image processing techniques were applied to the obtained speckle pattern images, and correlation analysis was performed. It has been observed that the CCs corresponding to the same stress values in the increasing and decreasing directions are in good agreement with each other. In this study, we created a CNN algorithm and trained this network with the data obtained from the sensors for different waist diameters and lengths. Our CNN can determine not only the strain quantity but also the direction of the applied strain with high precision and accuracy. The proposed sensor is a good candidate to measure not only strain but also physical quantities such as refractive index, temperature, pressure, and magnetic field in fiber sensor applications.

Acknowledgments

This study was supported by the Scientific and Technological Research Council of Turkey (TUBITAK), project no 121E248.

References

[1] R. Di Sante, L. Donati, E. Troiani, P. Proli, Metals and Materials International **20**, 537 (2014).
[2] H. Liu, Z. Zhu, Y. Zheng, B. Liu, F. Xiao, Optical Fiber Technology **40**, 144 (2018).
[3] R. Li, Y. Chen, Y. Tan, Z. Zhou, T. Li, J. Mao, Sensors **18**, 1607 (2018).
[4] Y.-J. Rao, Optical Fiber Technology **12**, 227 (2006).
[5] P. Xia, Y. Tan, C. Yang, Z. Zhou, K. Yun, Sensors **21**, 4989 (2021).
[6] Q. Li, J. Wang, H. Mu, J. Lv, L. Yang, Y. Shi, Z. Yi, P. K. Chu, Q. Liu, C. Liu, Opt. Commun. **527**, 128920 (2023).
[7] T. R. Woliński, P. Lesiak, A. W. Domański, Bulletin of the Polish Academy of Sciences, Technical Sciences **56**(2), 125 (2008).
[8] Zhaobing Tian, S. S.-H. Yam, IEEE Photonics Technology Letters **21**, 161 (2009).
[9] X. Dong, H. Du, Z. Luo, J. Duan, Sensors **18**, 278 (2018).
[10] X. Dong, H. Du, X. Sun, Z. Luo, J. Duan, Sensors **18**, 1549 (2018).
[11] S.-C. Her, C.-M. Yang, Sensors **12**, 3314 (2012).
[12] C. Liu, D. Sun, J. Yang, H. Zhang, L. Ran, Photonics **8**, 372 (2021).
[13] J. R. Ek-Ek, D. Jauregui-Vazquez, J. P. Korterik, M. Benedictus, F. Martinez-Pinon, H. L. Offerhaus, J. A. Alvarez-Chavez, Optical Fiber Technology **69**, 102843 (2022).
[14] C. Zhang, T. Ning, J. Zheng, J. Xu, X. Gao, H. Lin, J. Li, L. Pei, Opt. Laser Technol. **120**, 105687 (2019).
[15] R. Yang, Y.-S. Yu, C. Chen, Y. Xue, X.-L. Zhang, J.-C. Guo, C. Wang, F. Zhu, B.-L. Zhang, Q.-D. Chen, H.-B. Sun, Journal of Lightwave Technology **30**, 3126 (2012).
[16] M. Bilsel, I. Navruz, Advances in Electrical and Electronic Engineering **18**, 1.3545 (2020).
[17] E. Fujiwara, M. F. Marques dos Santos, C. K. Suzuki, Appl. Opt. **56**, 1585 (2017).
[18] D. Pal, S. Agadarov, Y. Beiderman, Y. Beiderman, A. Kumar, Z. Zalevsky, J. Biomed. Opt. **27**, 097001-1 (2022).
[19] A. R. Cuevas, M. Fontana, L. Rodriguez-Cobo, M. Lomer, J. M. Lopez-Higuera, Journal of Lightwave Technology **36**, 3733 (2018).
[20] F. Arı, H. Şerbetçi, İ. Navruz, Optical Fiber Technology **79**, 103366 (2023).
[21] E. Kakkava, B. Rahmani, N. Borhani, U. Teğin, D. Loterie, G. Konstantinou, C. Moser, D. Psaltis, Optical Fiber Technology **52**, 101985 (2019).
[22] U. Kürüm, P. R. Wiecha, R. French, O. L. Muskens, Opt. Express **27**, 20965 (2019).
[23] R. K. Gupta, G. D. Bruce, S. J. Powis, K. Dholakia, Laser Photon Rev. **14**, 202000120 (2020).
[24] Y. Li, Y. Xue, L. Tian, Optica **5**, 1181 (2018).
[25] H. Şerbetçi, I. Navruz, F. Ari, Ain Shams Engineering Journal 103122 (2024), in press, https://doi.org/10.1016/j.asej.2024.103122.
[26] R. Kumar, Sensors **22**(21), 8536 (2022).
[27] A. Ghaffar, Q. Li, I. Mehdi, K. Abro, N. Karim, C. C. Onyekwena, M. Mehdi, B. Chen, Optical Fiber Technology **67**, 102684 (2021).
[28] M. Wang, Q. Ma, L. Li, Z. Wang, B. Peng, Optical Fiber Technology **68**, 102779 (2022).

*Corresponding author: hserbetci@karatekin.edu.tr